RSC Advances

ROYAL SOCIETY OF CHEMISTRY

www.rsc.org/advances

Table of Contents Entry

Hierarchical self-assembly, photo-responsive phase behavior and variable tensile property of azobenzene-containing ABA triblock copolymers

Zai-Zai Tong, Jin-Qiao Xue, Rui-Yang Wang, Jie Huang, Jun-Ting Xu,* Zhi-Qiang Fan

MOE Key Laboratory of Macromolecular Synthesis and Functionalization, Department of Polymer Science & Engineering, Zhejiang University, Hangzhou 310027, China

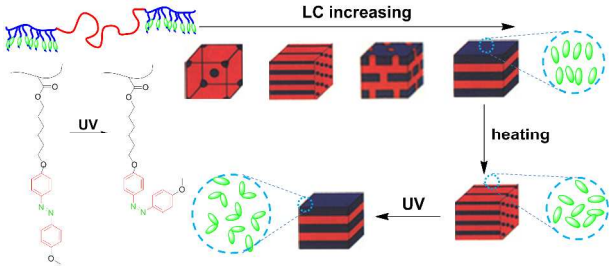

Journal Name

RSCPublishing

ARTICLE

Hierarchical self-assembly, photo-responsive phase behavior and variable tensile property of azobenzene-containing ABA triblock copolymers

Cite this: DOI: 10.1039/x0xx00000x

Received 00th January 2012,
Accepted 00th January 2012

DOI: 10.1039/x0xx00000x

www.rsc.org/

Zai-Zai Tong, Jin-Qiao Xue, Rui-Yang Wang, Jie Huang, Jun-Ting Xu,* Zhi-Qiang Fan

ABSTRACT: A series of triblock copolymers with liquid crystalline (LC) poly{6-[4-(4-methoxyphenylazo)phenoxy]hexyl methacrylate} (PMMAZO) as the end blocks and rubbery poly(*n*-butyl acrylate) (PnBA) as the midblock were synthesized. The effect of the interplay between the LC ordering and microphase separation on the hierarchical assembly of the triblock copolymers was studied. It is found that microphase separation at a larger scale can affect the LC ordering at a smaller scale, such as the stacking of the LC moieties, LC temperature and the domain size of the LC phase. On the other hand, alteration of the LC ordering, such as isotropization and sematic-to-nematic transition, may also lead to an order-order transition (OOT) or change in the long period of the microphase-separated structure. UV light can trigger the isomerization of the azobenzene LC moieties, which can be further amplified and exerts an effect on the microphase separation behavior, including the regularity of the microphase-separated structure and the OOT. The triblock copolymers also exhibit light-variable tensile property. The results reveal that the phase behavior and mechanical properties of this type of triblock copolymer can be readily regulated by light, thus it may be used as smart and functional thermoplastic elastomer.

1. Introduction

Block copolymers (BCPs), in which the different blocks are chemically linked, may produce a variety of ordered nanostructures such as lamellae (LAM), hexagonally perforated lamellae (HPL), gyroid (GYR), hexagonally packed cylindrical (HEX) and body-centered cubic spherical (BCC), through self-assembly or microphase separation.[1] Therefore, BCPs have a wide range of scientific and technological applications and have attracted lots of attention in past decades.[2-10] These nanostructures are formed as the system strives to balance between maximizing the conformational entropy and minimizing the interaction energy between the incompatible blocks.[7,11,12] The microphase-separated structures in BCPs are determined by the volume fraction f of the individual block and the segregation strength χN, which is the product of the Flory-Huggins interaction parameter χ and the polymerization degree N.[13] Because χ is inversely proportional to temperature, as a sample is heated, one may observe an order-disorder transition (ODT) corresponding to the loss of the ordered structure, or an order-order transition (OOT) corresponding to a transformation into another ordered structure. The microphase separation behavior of BCPs has been well understood through theoretical descriptions and experimental studies.[3,14]

Specifically, BCPs containing liquid crystalline (LC) blocks are more popular for the development of new functional materials due to the functionality of the LC blocks.[15-17] Hierarchical structures composed of the LC phase with a long period of 1-10 nm order and the microphase-separated domains with a long period of 10-100 nm can be formed in the LC block-containing BCPs.[10,18-23] It is reported that the LC ordering has a strong influence on the microphase behaviour of the LC-containing BCPs.[8,17,24-30] For example, the LC phase transition could trigger the phase transition of the microphase-separated structures of BCPs.[31-33] Hammond et al. observed that the ODT of a LC-containing BCP almost coincided with the clearing point of the LC block.[32] Moreover, the LC clearing transition can alter the interfacial curvature in the LC BCPs, resulting in an OOT of the microphase-separated morphology.[18,31,34] When the LC block is ordered, i.e. sematic or nematic, the microphase-separated structure prefers to be LAM or HEX rather than BCC with a highly curvatured

MOE Key Laboratory of Macromolecular Synthesis and Functionalization, Department of Polymer Science & Engineering, Zhejiang University, Hangzhou 310027, China
**Correspondence author. E-mail: xujt@zju.edu.cn , Tel./Fax: +86-571-87952400*

interface, even though the composition of BCP is quite asymmetric.[35-37] For an ABA triblock copolymer, in which B is a side-chain LC block, Sänger et al. observed that, upon heating, the LC isotropization caused an OOT from BCC to HEX.[31] The isotropization of the LC microdomains may also cause the change in macroscopic properties, such as the mechanical properties, though the microphase-separated morphology remains unchanged.[38]

Azobenzene-containing polymers are of great interest since the azobenzene chromophore can undergo reversible *trans-cis* photoisomerization.[39-44] The azobenzene chromophore can act both as photo-responsive moiety and LC mesogen.[45,46] Usually, the azo-group with a *trans* configuration can form a LC phase, since the *trans*-isomer is rod-like. Upon UV irradiation, the azobenzene moiety tends to produce a *cis*-isomer, which cannot form a LC phase due to its bent shape, concomitantly with isotropization of the LC phase.[45,47] The photoresponsive property of the azobenzene moiety affords good light-controllability to the azobenzene-containing polymers.[48-50] For example, in the azobenzene-containing BCPs the photoisomerization of azobenzene can lead to the change in microphase separation of the BCPs in the bulk[12,51,52] and orientation of the microphase-separated domains in the thin film.[12,53] The *trans-cis* photoisomerization of the azobenzene moiety may also results in the macroscopic contraction in size.[54,55] This striking photomechanical effect arises from the photoselective volume contraction.[56,57]

Although lots of researches have been carried out on the photoresponsive behavior of azobenzene-containing polymers and BCPs, following three aspects still need further exploration. (1) It is widely reported that the LC ordering can affect the microphase separation behaviour.[8,17,24-30] However, we believe that in a hierarchically self-assembled system there may exist interplay between the structures at different scales. As a result, a question is raised: Can microphase separation affect the LC ordering? (2) The effect of the LC ordering on the microphase-separated morphology, ODT and orientation of the microdomains has been reported,[12] but the OOT of the microphase-separation structure triggered by the change of the LC ordering is seldom observed. If we can achieve this, it means that we can switch between different ordered microphase-separated structures by alteration of the LC ordering. (3) Photoisomerization of the azobenzene moiety usually leads to a volume change and thus deformation of the azobenzene-containing materials.[54,55] Nevertheless, the change of mechanical properties induced by photoisomerization is more interesting and worthy studying. In this work, we prepared a series of ABA-type azobenzene-containing triblock copolymers, with poly{6-[4-(4-methoxyphenylazo)phenoxy] hexyl methacrylate} (PMMAZO) bearing the azobenzene moiety in the side chain as the A end blocks and poly(*n*-butyl acrylate) (PnBA) as the B central block. In these triblock copolymers, the central P*n*BA block is rubbery and accounts for the major volume fraction, and the PMMAZO end blocks are rigid and can act as physically cross-linking points. As a result, these PMMAZO-*b*-PnBA-*b*-PMMAZO triblock copolymers are a type of thermoplastic elastomer (TPE). Our emphasis was put on the interplay of LC ordering and microphase separation, LC ordering triggered OOT and the effect of UV radiation on the microphase behavior and mechanical properties of PMMAZO-*b*-PnBA-*b*-PMMAZO BCPs. Our results demonstrated that the phase behavior and mechanical properties of the PMMAZO-*b*-PnBA-*b*-PMMAZO triblock copolymers could be regulated with UV irradiation and thus they are candidates as a smart and functional TPE material.

2. Experimental section

2.1. Materials

Tetrahydrofuran (THF) was refluxed with sodium and distilled. *n*-Butyl acrylate (nBA) was washed with 10 wt% sodium hydroxide and deionized water for 3 times, then dried with calcium hydride overnight and distilled under vacuum before use. Copper bromide was washed with acetic acid and diethyl ether for several times and dried under vacuum. The other commercially available chemicals were used without further purification. The monomer of 6-[4-(4-methoxyphenylazo)phenoxy]hexyl methacrylate (MMAZO) was synthesized according to the procedure reported in literature.[58,59]

2.2. Synthesis of macroinitiator and triblock copolymers

The synthesis of poly(n-butyl acrylate) (PnBA) was given below as an example. In a Schlenk flask, diethyl meso-2,5-dibromoadipate (15.8 mg), n-butyl acrylate (5.0 mL), *N,N,N′,N′,N″*-pentamethyldiethylenetriamine (PMDETA) (15 μL), toluene (1.0 ml) were mixed and stirred for 10 min. The mixture was immediately frozen in liquid nitrogen, and a vacuum was applied. After 3 freeze-thaw cycles, CuBr (6.3 mg) was added under N_2, then the flask was put in an oil bath at 70 °C for polymerization. After reaction for 20 h, the content in the flask was dissolved in THF and passed through an alumina column to remove the metal complex. After being concentrated, the THF solution was precipitated in water/methanol (1:1). The purification by dissolving and precipitation was repeated several times.

A typical procedure for synthesis of the triblock copolymers was described as follows in detail. A Schlenk flask with a stir bar was charged with 495 mg of PnBA (macroinitiator for the midblock), 446 mg of MMAZO, 21 μL of PMDETA and 4 mL of THF. The mixture was stirred for 10 min to form homogenous solution. The mixture was frozen under liquid N_2 and 3 freeze-thaw cycles was performed. 6.0 mg of CuBr was introduced under N_2 atmosphere. The flask was put in an oil bath at 60 °C to conduct polymerization for 10 h. The reaction mixture was dissolved in THF and passed through an alumina column to remove Cu salt. The solution was then concentrated and precipitated in methanol repeatedly to purify the product.

2.3. Characterizations

Molecular weight and polydispersity index (PDI) were characterized by gel permeation chromatography (GPC) using a Waters system calibrated with standard polystyrenes. THF was

used as an eluent at a flow rate of 1.0 mL min^{-1}. ^1H NMR spectra were recorded on a Bruker DMX-400 MHz. The glass transition temperature (T_g) and LC phase transition temperatures were measured on differential scanning calorimetry (DSC, TA Q200) with a heating rate of 10 °C min^{-1}. Polarized optical microscopy (POM) observations were carried out on an Olympus microscope (BX51) equipped with a hot stage. Samples for wide angle X-ray diffraction (WAXD) and small angle X-ray scattering (SAXS) were cut from compression-molded film. The WAXD and SAXS experiments were performed at BL14B and BL16B1 beamlines, respectively, in Shanghai Synchrotron Radiation Facility (SSRF) in China. The wavelength of the X-ray source was 1.24 Å. The sample-to-detector distance was set as 405 mm for WAXD experiments, while 1900 mm for SAXS experiments. The 2D patterns were converted into one-dimensional (1D) profiles using Fit2D software. Transmission electron microscope (TEM) observations were carried out on a JEOL JEM-1200EX instrument at an acceleration voltage of 90 kV. The ultrathin films for TEM observation were prepared from the compression-molded films at -80 °C with a microtome machine. The samples were stained with OsO_4 vapor before TEM observation. The UV-Vis spectra of the BCP thin film on a clean, UV-transmitted quartz slide, were measured by using a Cary 100 UV-Vis. Irradiation with UV light (365 nm) of the thin film were performed on a UV-lamp (45 mW cm^{-2}). The stress-strain behavior under uniaxial tension was performed on a CMT 4204 instrument at 25 °C. The tensile specimens were cut from the compression molded films with the thickness of about 0.2 mm. The distance of two grips was 15 mm and the specimen width was 2 mm. A strain rate of 5 mm min^{-1} was applied to uniaxial tension. The UV-responsive tensile experiment was performed in a UV light environment with an intensity of 45 mW cm^{-2}. The samples were exposed in UV at room temperature for 30 min before drawing.

3. Results and discussion

3.1. Polymerization result

Atom transfer radical polymerization (ATRP) was used to prepare the azobenzene-containing triblock copolymers. The synthetic rout of the PMMAZO-*b*-PnBA-*b*-PMMAZO block copolymer is described in Scheme 1 in detail. Diethyl meso-2,5-dibromoadipate was selected as the initiator to synthesize the macroinitiator (Br-PnBA-Br). Three kinds of central block, Br-PnBA-Br, with different molecular weights were synthesized and thus a series of triblock copolymers with various amounts of end LC block were prepared. Since in TPEs the end blocks acting as physically crosslinking points should have a high T_g, the methacrylic monomer, instead of acrylic monomer, was chosen to fabricate the end blocks. The obtained triblock copolymers were characterized by GPC, ^1H NMR and DSC (Fig. S1 and S2), and the structural information is summarized in Table 1.

The content of the LC block (minor component) is controlled by the conversion of MMAZO monomer, and the PMMAZO content ranges from 15 wt% to 47 wt%. It should be noted that,

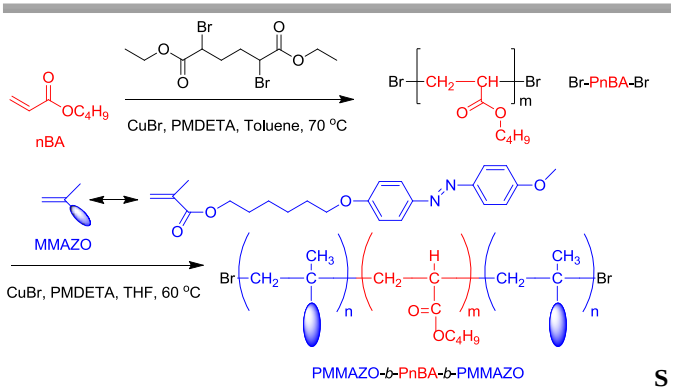

Scheme 1 The synthetic route of the PMMAZO-*b*-PnBA-*b*-PMMAZO triblock copolymers.

Table 1 Characteristics of synthesized polymers

Sample	M_n^{GPC}	PDI	Composition (NMR)[a]	Conv[b] (%)	LC content[b] (wt%)	T_g (°C)	T_{S-N}[c] (°C)	T_{N-I}[d] (°C)
PnBA-1	26100	1.14	$PnBA_{204}$			-51		
P1	31800	1.12	$PMMAZO_8$-*b*-$PnBA_{204}$-*b*-$PMMAZO_8$	21.4	19.5	-48	84.2	117.1
P2	36600	1.14	$PMMAZO_{18}$-*b*-$PnBA_{204}$-*b*-$PMMAZO_{18}$	47.6	35.3	-47	92.7	130.7
P3	39900	1.13	$PMMAZO_{21}$-*b*-$PnBA_{204}$-*b*-$PMMAZO_{21}$	53.6	38.9	-47	93.3	131.3
P4	43600	1.20	$PMMAZO_{29}$-*b*-$PnBA_{204}$-*b*-$PMMAZO_{29}$	75.0	46.8	-46	94.3	133.0
PnBA-2	56900	1.10	$PnBA_{445}$			-48		
P5	72900	1.17	$PMMAZO_{29}$-*b*-$PnBA_{445}$-*b*-$PMMAZO_{29}$	41.6	28.6	-47	94.8	134.9
P6	81600	1.23	$PMMAZO_{41}$-*b*-$PnBA_{445}$-*b*-$PMMAZO_{41}$	50.8	36.5	-47	95.7	135.8
PnBA-3	72300	1.10	$PnBA_{564}$			-47		
P7	83600	1.12	$PMMAZO_{16}$-*b*-$PnBA_{564}$-*b*-$PMMAZO_{16}$	26.3	14.9	-47	93.9	134.2
P8	90400	1.18	$PMMAZO_{29}$-*b*-$PnBA_{564}$-*b*-$PMMAZO_{29}$	48.0	24.1	-47	95.3	135.7
P9	96600	1.17	$PMMAZO_{42}$-*b*-$PnBA_{564}$-*b*-$PMMAZO_{42}$	68.9	31.4	-46	95.5	136.1

[a] Using GPC-determined central block. [b] determined from ^1H NMR. [c] The transition temperature from sematic state to nematic state. [d] The transition temperature from nematic state to isotropic state.

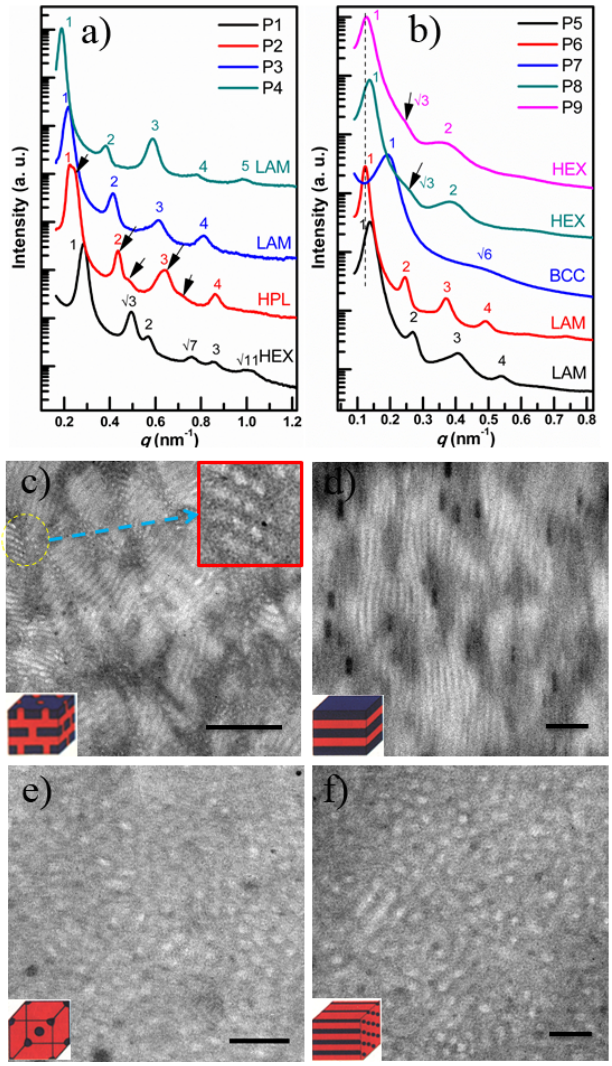

Fig.1 SAXS measurement and TEM observation for triblock copolymers: (a) SAXS profiles of P1-P4 and (b) P5-P9; selected TEM micrographs of (c) P2, inside is the magnification of the dashes circle; (d) P5; (e) P7; (f) P9. The scale bar in the figures is 200 nm. The samples were annealed at 150 °C for 24 h before measurements.

because we attempt to use the PMMAZO-*b*-PnBA-*b*-PMMAZO triblock copolymers as TPE, the BCPs with PMMAZO as the minor component were prepared. It is found that all the triblock copolymers have a narrow polydispersity. However, a weak shoulder peak can be observed in the GPC curves of the samples P5-P9 when the PnBA central block has a high molecular weight (Fig. S1). The shoulder peak corresponds to a molecular weight that is about twice of the main peak, implying that coupling termination reaction may readily take place at high molecular weight. It seems difficult to avoid such a side reaction at high molecular weight, since similar result was also reported by others.[38,60]

3.2. Self-assembled hierarchical structures at room temperature

Before characterization by various techniques, all the triblock copolymers were annealed at a temperature higher than the isotropization temperature (T_{N-I}) of the LC PMMAZO blocks (150 °C) for 24 h in vacuum to ensure full microphase separation. Subsequently, the BCPs were cooled to room temperature to allow the LC ordering inside the microphase-separation domains. Firstly the microphase-separated structures of the PMMAZO-*b*-PnBA-*b*-PMMAZO triblock copolymers at room temperature were characterized by SAXS and TEM. Fig. 1a and 1b show the SAXS profiles of P1-P9 at room temperature. The samples P1-P4 with a low molecular weight central block form a variety of different ordered nano-structures with increasing the amount of PMMAZO block. For example, when the content of PMMAZO block is 19.5 wt% (P1), the relative scattering vector of the SAXS peaks to the first-order peak, q/q^*, is 1:√3:2:√7:3:√11, which indicates a HEX structure. As the PMMAZO content is increased to 35.3 wt% (P2), seven scattering peaks are discernable in the SAXS profile. Two series of q/q^* are observed: one is 1:2:3:4 and the other is 1:√3:2:√7:3 (indicated by the black arrows in Fig. 1a). The former represents a LAM structure and the latter corresponds to a HEX structure. As a result, we speculate that HPL structure or a mixed structure of LAM and HEX is formed in P2. The morphology of P2 is further examined by TEM (Fig. 1c). One can see that the lamellar microdomains are the majority. However, some cylindrical microdomains can be observed as well. As shown in the red box of Fig. 1c, the microdomains are hexagonally packed when the sample is cut along the direction normal to the long axis of the cylinders. Based on the TEM image and SAXS profile, it can be recognized that the P2 should have a HPL structure at room temperature. Further increasing the length of the PMMAZO block leads to the formation of a LAM structure, as revealed by the relative position of various SAXS peaks. The LAM structure in P4 is confirmed by TEM, as shown in Fig. S3a of supplementary material.

The samples P5 and P6 with an intermediate molecular weight central block form a LAM structure, even though the PMMAZO content in P5 is as low as 28.6 wt%. The LAM structure of P5 can be confirmed by both the SAXS profile, in which the value of q/q^* is 1:2:3:4, and TEM image (Fig. 1d). It should be noted that, P2 has a higher PMMAZO content than P5, but P2 exhibits a HPL structure. This can be attributed to the different polymerization degrees of P5 and P2. Since the segregation strength of a BCP is determined by the parameter χN, a higher N will result in a larger χN. Therefore, although the PMMAZO content of P5 is lower than that of P2, formation of the LAM structure in P5 is reasonable, which can be seen from the phase diagram of BCPs.[3]

The microphase-separated structures of the samples P7-P9 with a high molecular weight central block were characterized as well. In the SAXS profile of P7, a broad high-order peak appears at $q/q^*=\sqrt{6}$ besides the first-order peak but no other high-order peaks are observed. This indicates that the structure of P7 is not well ordered. Spherical microdomains are observed in the TEM micrograph of P7. In combination of the SAXS profile with the TEM micrograph, we can conclude that P7 has though the high-order peaks are not so sharp (Fig. 1b). Both

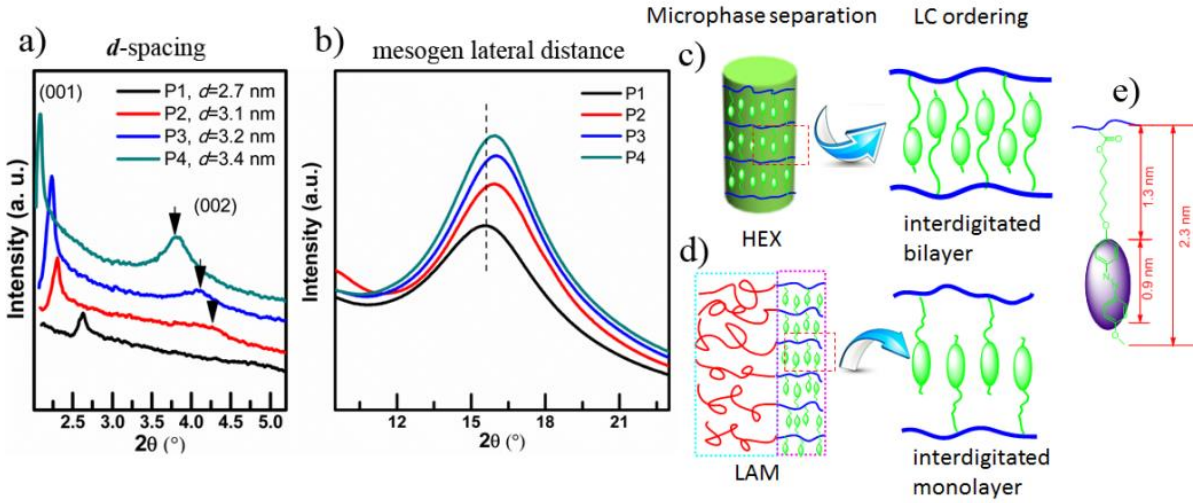

Fig.2 WAXD patterns of P1-P4 samples at room temperature at low angle reflecting the *d*-spacing (a), and at large angle reflecting lateral distance of the LC moieties (b). The arrows show the second-order diffraction peak. Illustrations of hierarchical structures from microphase-separated structure to the stacking of the LC moieties for P1 (c) and P4 (d). Side chain structure and length of the PMMAZO block (e).

rod-like and spherical microdomains can be observed in the TEM image of P9, as shown in Fig. 1f. As a result, a HEX structure is formed in P8 and P9. As compared with P5, P9 has both a higher molecular weight, i.e. a larger χN, and a higher PMMAZO content. Nevertheless, P9 forms a HEX structure while P5 forms a LAM structure. This is difficult to understand in terms of the phase diagram of BCPs. Usually, a BCP with a larger χN and a higher volume fraction of the minor component tends to form a LAM structure more easily, rather than a HEX structure. Such a result may be explained by the presence of a small amount of high molecular weight fractions in P7-P9, which are produced by the coupling termination side reaction (Fig. S1). It is reported that increase in polydispersity may drive morphological transitions, including LAM-to-GYR and GYR-to-HEX transitions,[61] and lead to an abnormal phase diagram.[62] Herein these high molecular weight fractions may exert some effects on the phase behavior of PMMAZO-*b*-PnBA-*b*-PMMAZO triblock copolymers. They may also be responsible for the less ordered structures in P7-P9.

The structure of the LC phase inside the microphase-separated domains was characterized with WAXD. Fig. 2a and 2b show the room temperature WAXD patterns of the samples P1-P4 at low and large angles, respectively. One can see that, as the PMMAZO content increases, the first-order peak of the LC phase shifts to lower angle, indicating a large *d*-spacing. The *d*-spacings of these four samples calculated from Bragg equation are indicated in Fig. 2a. Moreover, for the sample P2, a weak peak at large angle (indicated by the arrow) becomes visible. Since the reciprocal spacing of the first peak is twice of the second peak, they are likely the first- and second-order diffractions from the same lamellar stacking of the PMMAZO blocks. For P3 and P4, the second-order peak becomes more obvious, indicating a more ordered lamellar arrangement of the LC moieties. The arrangement of the LC moieties can be further inferred by comparing the experimentally determined *d*-spacings with the calculated ones. Generally, the LC moieties can be stacked into bilayer, interdigitated bilayer and interdigitated monolayer, depending on the structure of molecules, as reported in the literature.[21,22,63,64] The azobenzene moieties are in the side-chain of MMAZO, and the length of the side-chain can be calculated by ChemDraw software, which is shown in detail in Fig. 2e. The *d*-spacing of P1 is 2.7 nm, which is larger than the full length of the extended side chain. The most probable model for the stacking of the LC moieties in P1 is the interdigitated bilayer structure, as depicted in Fig. 2c. According to this model, the calculated *d*-spacing is 2.3 + (1.3-1.0) =2.6 nm, which is similar to the measured value. By contrast, the *d*-spacing of P4 (3.4 nm) is evidently larger than the length of the side-chain of MMAZO, but smaller than twice the length of the side-chain. We proposed an interdigitated monolayer structure for the arrangement of the LC moieties in P4, as illustrated in Fig. 2c. In such a structure, the calculated *d*-spacing is about 1.3×2+0.9=3.5 nm, which is comparable to the value experimentally determined by WAXD. The *d*-spacings of P2 and P3 are between those of P1 and P4, indicating that the stacking structure of the LC moieties in these two samples changes gradually from the interdigitated bilayer into interdigitated monolayer, as the PMMAZO content increases. We also examined the LC ordering in P5-P9. As shown in Fig. S4 of supplementary material, the LC ordering in the BCC domains is rather weak, while in the HEX or LAM domains it is similar to that in P1-P4.

On the other hand, a typical broad halo at large angle (2θ~16°, *d*~0.45 nm) is observed for all the studied samples, which is attributed to the lateral distance between the azobenzene moieties. It is found that the lateral distance of P1 is slightly larger than other samples. Since the LC ordering of P1 is confined in the HEX microdomains, which have a larger curvature at the interface than the HPL and LAM structures, the azobenzene moieties are not so closely stacked. This result is

also consistent with the low diffraction intensity of the first-order peak that reflects the LC ordering in P1 (Fig. 2a).

Above result reveals that the LC ordering at a smaller scale varies with the microphase-separated structure at a larger scale. The LC moieties are well stacked into interdigitated monolayers in the lamellar microdomains, while they tend to be loosely arranged into interdigitated bilayers in the cylindrical microdomains. This difference possibly arises from the different curvatures of the interface in the LAM and HEX structures.

The LC phase transition and the macroscopic morphology of the PMMAZO-*b*-PnBA-*b*-PMMAZO triblock copolymers were characterized with DSC and POM. Fig. 3a shows the second run DSC heating curves of P1-P4 as well as the PnBA-1 macroinitiator. The DSC curves for the other samples are presented in Fig. S5 of supplementary material. The low glass transition temperature of the PnBA macroinitiator (~ -50 °C) almost remains unchanged in all the BCPs (Table 1), indicating a thorough microphase separation of the PMMAZO and PnBA blocks. On the other hand, the PMMAZO block displays two mesophase transitions. Usually PMMAZO exhibits a sematic A LC structure at room temperature.[65] Upon heating, the sematic A phase first transforms into a nematic phase and the transition temperature is indicated as $T_{S\text{-}N}$. When it is further heated, the nematic phase may become isotropic at a transition temperature of $T_{N\text{-}I}$. All the triblock copolymers form a lamellar sematic A LC phase at room temperature, as revealed by the WAXD patterns (Fig. 2a and 2b). Following the assignments in the neat PMMAZO and other PMMAZO-containing BCPs,[66] we believe that the two transition temperatures in the PMMAZO-*b*-PnBA-*b*-PMMAZO triblock copolymers observed by DSC also correspond to $T_{S\text{-}N}$ and $T_{N\text{-}I}$. The LC phase transition temperatures of $T_{S\text{-}N}$ and $T_{N\text{-}I}$ are summarized in Table 1. One can see from Fig. 3a that the $T_{S\text{-}N}$ and $T_{N\text{-}I}$ of P1 is obviously lower than those of P2-P4. This agrees well with the WAXD result and is due to the lower PMMAZO content and less ordered LC phase in P1. For the PMMAZO content increases. A similar trend is observed for the other two series of triblock copolymer, P5-P6 and P7-P9 (Table 1).

The morphology evolution of the P4 upon heating was monitored by POM. The POM micrographs at indicated temperatures are shown in Fig. 3b-e. We can observe that the textural structures below and above 90 °C are different to some extent, and there is no birefringent texture above 130 °C. The two-step transition of the textural structure agrees well with the two transition temperatures observed by DSC. Unfortunately, the typical grainy texture, which exists in the PMMAZO homopolymers (Fig. S6 in supplementary material), can hardly be identified in the BCPs. It may be due to that the development of the LC domains into large size is hindered by the microphase-separated structure. As a result, we cannot determine the textural structures of the PMMAZO-*b*-PnBA-*b*-PMMAZO triblock copolymers by POM. Above results demonstrate that the microphase-separated structure at a larger scale can affect the LC ordering at a smaller scale, including the stacking of the LC moieties, the LC phase transition temperature and the domain size of the LC phase, which is rarely reported in literature.

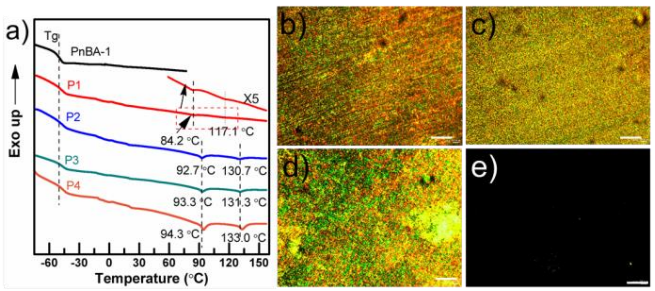

Fig. 3 The second run DSC heating curves of P1-P4 (a) and POM images of P4 during the heating process at 25 °C (b), 90 °C (c), 130 °C (d) and 150 °C (e), respectively. The scale bar in the figures is 50 μm.

3.3. Effect of the LC ordering on microphase separation

On the other hand, it is reported that the LC ordering may also affect the microphase separation behavior. In order to reveal such an effect, the evolution of the microphase-separated morphology during the LC phase transitions was monitored with temperature-variable SAXS. The representative SAXS profiles of P1-P4 at various temperatures are compiled in Fig. 4. The SAXS profiles of the other samples are supplied in Fig. S7 of supplementary material. In order to avoid decomposition of the BCPs, the temperature for SAXS measurement should not exceed 200 °C. For the sample P1, the scattering vector ratio of different SAXS peaks is always $1:\sqrt{3}:2:\sqrt{7}$ at temperature below 150 °C, although the high-order peaks become weaker as temperature increases (Fig. 4a). This shows that the microphase-separated structure is always HEX when the structure of the LC phase changes from sematic A into nematic, then into isotropic upon heating, and the LC ordering has an insignificant effect on microphase separation in this sample. P1 becomes disordered when temperature is above 150 °C. For the sample P2, we observe an OOT from HPL to HEX at 110 °C upon heating (Fig. 4b). However, since this temperature does not correspond to any transition of the LC phase, such an OOT is simply caused by the decrease of χ with increasing temperature, which is frequently observed in common BCPs. The T_{ODT} of P2 is 170 °C, as shown in Fig. 4b. By contrast, when heating the sample P3, an OOT from LAM to HEX is observed at 130 °C (Fig. 4c). Since such a temperature is quite close to the $T_{N\text{-}I}$ of P3, we believe that isotropization of the LC phase causes the observed OOT in P3, which is similar to the result reported by Säanger et al..[31] However, the possibility that the OOT from LAM to HEX is due to decrease of χ with increasing temperature cannot be completely excluded. As for the sample P4, the scattering vector ratio is always 1:2:3:4 in the studied temperature range, indicating no change in the microphase-separated structure. On the other hand, the long period (L) of the microphase-separated structure also varies with temperature. As can be seen from Fig. 4e, the L decreases more sharply around the LC phase transition temperatures.

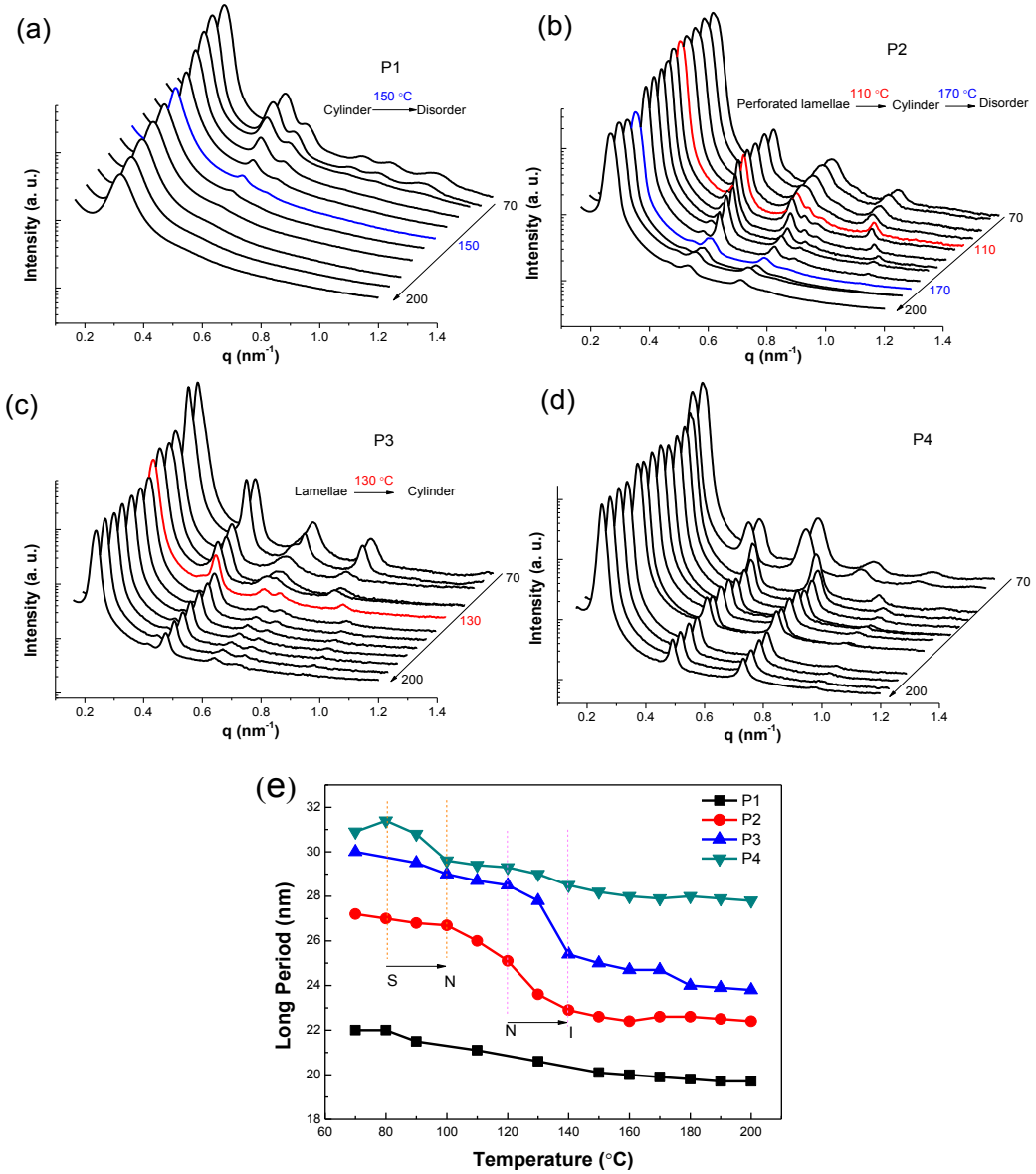

Fig. 4 Temperature-variable SAXS profiles of P1 (a), P2 (b), P3 (c) and P4 (d) and variation of the long period (L) with temperature for the samples P1-P4 (e).

Such a phenomenon is particularly obvious around the $T_{N\text{-}I}$ of P2 and P3, and $T_{S\text{-}N}$ of P4. This is possibly because the phase transition of the LC phase is usually concomitant with the volume change of the microdomains.

The temperature-variable SAXS results show that the isotropization of the LC phase can affect the microphase separation behavior of PMMAZO-*b*-PnBA-*b*-PMMAZO triblock copolymers with a specific composition, such as P3. This implies that the effect of LC ordering at a smaller scale on microphase separation at a larger scale is limited and it takes effect only when the composition of the BCPs is located near the boundary of two microphase-separated structures. OOT is usually observed for a given BCP when χ changes. Temperature is the main factor affecting χ. The isotropization of the LC phase may also lead to change of χ. In the LC state, there is a strong interaction among the LC moieties, which alienates the PMMAZO block from the PnBA block, thus the value of χ between the two blocks is larger. After isotropization, the interaction among the LC moieties becomes weaker, whereas the interaction between the PMMAZO block from the PnBA block may become stronger, resulting in a decreased χ and thus the OOT of LAM-to-HEX in P3. Moreover, isotropization can facilitate the elastic deformation of the LC phase, which allows the BCPs to form a microphase-separated structure with a highly curvatured interface, such as HEX. Therefore, the variations of the hierarchical self-assembly structures of PMMAZO-*b*-PnBA-*b*-PMMAZO with composition and temperature show that there exists interplay between the LC ordering at a smaller scale and microphase separation at a larger scale.

3.4. UV irradiation-triggered phase transition

Since the azobenzene LC moiety is photoresponsive, we also try to use light to induce the isomerization of the LC moieties and study its effect on the microphase separation behavior of PMMAZO-*b*-PnBA-*b*-PMMAZO BCPs. The photoisomerization of azobenzene in thin film (~10 μm) of P3 was first monitored by UV-Vis spectroscopy, as shown in Fig. 5. Upon irradiation with UV light at 365 nm the absorption band at around 355 nm decreases remarkably, and concomitantly the band at around 468 nm increases slightly. The absorption bands at 355 and 468 nm are ascribed to π-π* and n-π* transitions, respectively.[67,68] The change of the absorption bands induced by UV irradiation is indicative of the photoisomerization of azobenzene moieties from the *trans*- to the *cis*-state. After exposure to UV irradiation for 15 min, the *trans* isomers almost change into *cis* ones, since prolonging the exposure time (30 min) has no effect on the UV-Vis spectrum (not shown here). After absorption of UV light, the azobenzene moieties isomerize into a metastable *cis* state. The *cis* isomers can be switched back to the *trans* ones by visible light. On the *trans-cis* conversion, the azobenzene moieties change their molecular shape and the distance between the *para*-positions is reduced from 9 to 5.9 Å. Consequently, photoisomerization of the azobenzene moieties enriches the conformation of the PMMAZO blocks and leads to a gain in entropy and a smaller density.

Since in the LC block-containing BCPs the structure at a smaller scale may affect the structure at a larger scale, it is expected that the microphase separation behavior of PMMAZO-*b*-PnBA-*b*-PMMAZO triblock copolymers may be regulated by light. Fig. 6 shows SAXS profiles before and after UV irradiation for some selected samples (P1 and P3) at indicated temperatures. It is found that there is no significant difference between the SAXS profiles of P1 at 40 °C before and after UV irradiation (Fig. 6a). This can be attributed to the glassy state of the PMMAZO block (T_g: ~73 °C, as shown in Fig. S8), which may freeze the microphase-separated structure, although the azobenzene moieties in the side chains of the PMMAZO blocks can undergo *trans-cis* isomerization at room temperature. As a result, we raise the temperature to 130 °C. At this temperature, both the first- and second-order SAXS peaks of P1 become diffused and the third-order peak at q/q^* =2

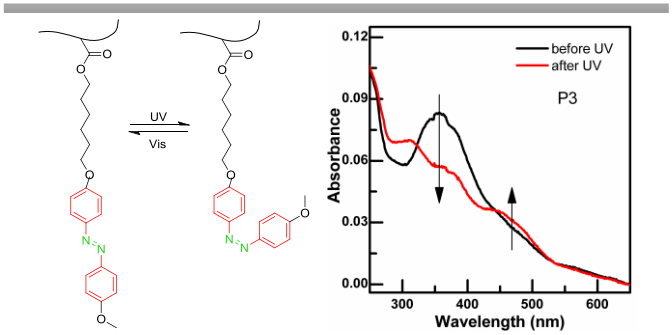

Fig. 5 (a) Scheme for reversible photoisomerization of the azobenzene moieties upon irradiation with UV and visible light, respectively. (b) UV-Vis absorption spectra of P3 thin film on a clean, UV-transmitted quartz slide before and after exposure to UV light with a wavelength of 365 nm and an intensity of 45 mW cm^{-2} for 15 min at room temperature.

disappears after UV irradiation, though the HEX structure of the microphase-separated morphology seems unchanged (Fig. 6b). This indicates that UV irradiation may reduce the regularity of the microphase-separated structure. In other words, the T_{ODT} of P1 may be lowered by UV irradiation. It should be pointed out that the experimental temperature is higher than the T_{N-I} of P1 (117.1 °C) and the PMMAZO microdomains are isotropic at 130 °C. Therefore, the change in microphase separation behavior of P1 upon UV irradiation is simply caused by the photoisomerization of the azobenzene moieties, instead of the phase transition of the LC phase.

Fig. 6c shows the SAXS profiles of P3 before and after irradiation at 130 °C. As revealed in Fig. 4c, the microphase-separated structure of P3 is transformed from LAM at low temperature into HEX at 130 °C due to isotropization by heating. After UV irradiation, the scattering peaks at $q/q^*=\sqrt{3}$ and $\sqrt{7}$ disappear and the scattering vector ratio of different SAXS peaks is 1:2:3:4, which indicates a LAM structure. This shows that UV irradiation at 130 °C can drive the microphase-separated structure of P3 back to LAM.

As we can see that, photoisomerization of the LC moieties may affect the regularity or cause an OOT of the microphase-separated structure. The reduction in regularity of the microphase-separated structure by UV irradiation is due to the decrease of χ between the two blocks. Because the *cis*-isomers of the LC moieties are stacked not as regularly as the *trans*-isomers, the interaction among the PMMAZO blocks is weakened, and thus the value of χ between the two blocks is reduced, as mentioned in the previous section. However, the OOT of HEX-to-LAM in P3 induced by UV irradiation cannot be attributed to the decrease of χ, since an OOT from LAM to HEX, instead of from HEX to LAM, is usually observed as χ decreases. Moreover, since the azobenzene moieties in P3 are already isotropic at 130 °C, there is no big difference in the elastic deformability between the *cis*- and *trans*-isomers, and the possibility that the alteration in the elastic deformability of the azobenzene moieties after isomerization causes the OOT of P3 can be excluded as well. Even though this factor takes effect, *cis*-isomers with a bent shape are advantageous to formation of the structure with a highly curvatured interface, such as HEX. We ascribe the OOT of P3 upon UV irradiation to the change in volume fraction of the PMMAZO blocks. Isomerization due to UV irradiation leads to a more loose arrangement of the *cis*-isomers, thus the volume fraction of the PMMAZO blocks is enhanced. As pointed out in the previous section, the sample P3 may have a composition near the boundary of two microphase-separated structures, a slight change in χ induced by isotropization upon heating or volume fraction by isomerization may result in an OOT of the microphase-separated structure, which can be illustrated in Scheme 2. On the one hand, isotropization by heating mainly causes a decrease in χ, which drives an OOT of LAM-to-HEX. On the other hand, isomerization by UV irradiation mainly leads to a decrease in density, which is responsible for the OOT of HEX-to-LAM. This shows that, for a PMMAZO-*b*-PnBA-*b*-PMMAZO BCP with a suitable composition, we may switch between different

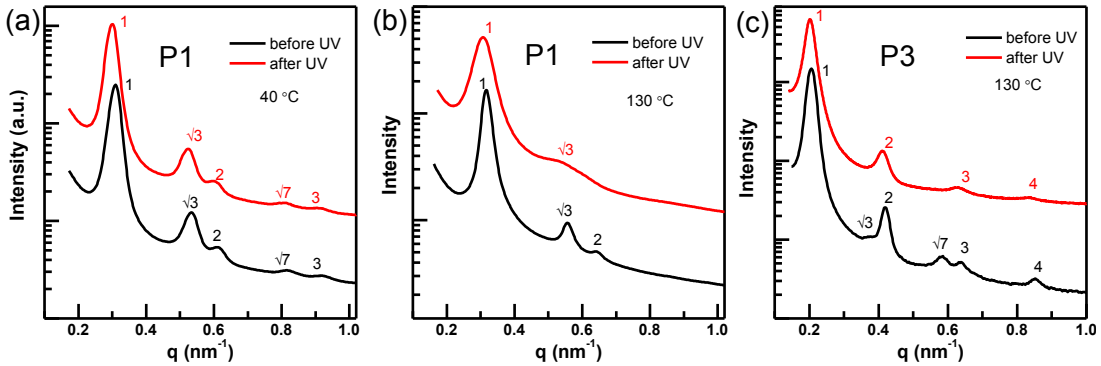

Fig. 6 SAXS profiles of different samples before and after UV irradiation. (a) P1 at 40 °C; (b) P1 at 130 °C and (c) P3 at 130 °C. The thin films were first exposed to UV light with a wavelength of 365 nm (45 mW cm^{-2}) for 30 min at the indicated temperature and then SAXS measurements were carried out under UV irradiation.

ordered microphase-separation structures by adjusting the LC ordering through temperature change or UV irradiation. It should be noted that isotropization and isomerization have opposite effects on the microphase separation behavior. As a consequence, when P3 is irradiated with UV light at lower temperature (125 °C), at which a LAM structure is formed, isotropization and isomerization take place simultaneously. These two factors will counteract each other and no OOT is observed.

3.5. Effect of UV irradiation on tensile behaviors

As we can see, the configuration of the azobenzene moieties and the microphase-separated structure of the PMMAZO-*b*-PnBA-*b*-PMMAZO BCPs may be changed after UV irradiation, thus the mechanical properties may also be regulated by light irradiation. Since the mechanical properties of TPEs strongly depend on the molecular weight and the content of the physically cross-linking points, the samples P5 and P8 with high molecular weights and larger PMMAZO contents are selected for the tensile drawing test. The uniaxial stress-strain curves of P5 and P8 at room temperature before and after UV irradiation are illustrated in Fig. 7. The tensile curves of P6 and P9 without UV irradiation are shown in Fig. S9. Since the sample P7 has a low PMMAZO content and the physically cross-linking points are too few, it shows no elasticity.

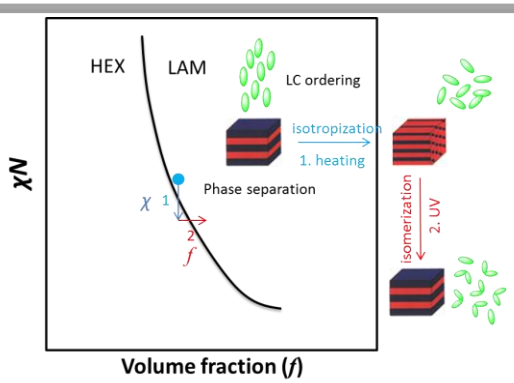

Scheme 2 Illustration for the effects of χ induced by isotropization and volume fraction, *f*, induced by UV irradiation on OOT of P3.

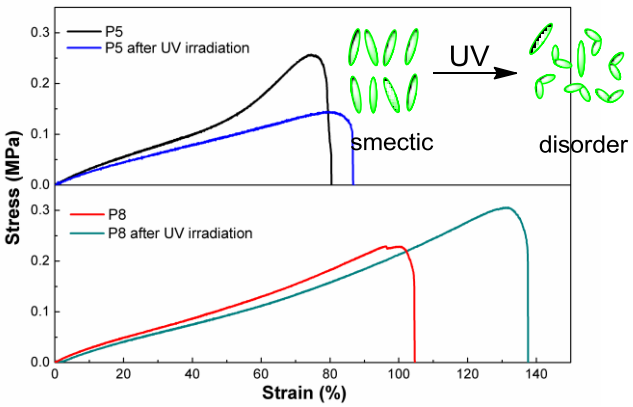

Fig. 7 The uniaxial stress-strain curves of P5 and P8 at room temperature before and after UV irradiation.

It is observed that P5 exhibits a stress-strain behavior with typical characteristics of elastomers, i.e. diffused yielding point upon deformation. The stress increases steadily in the initial period of tensile drawing and strain-hardening occurs with a larger slope at the late stage. The strain at break of P5 can reach 80%. Such a stress-strain curve agrees with the structure in P5 that the plastic microdomains are dispersed in the rubbery matrix. After UV irradiation, the strain at break of P5 becomes slightly larger (90%), but the strain-hardening phenomenon at large strain can hardly be observed, and the tensile strength at break is remarkably reduced. On the other hand, as compared with P5, the sample P8 shows a larger strain at break but the strain-hardening phenomenon is not so pronounced in P8. This can be attributed to the lower PMMAZO content and higher molecular weight of P8. After P8 is irradiated with UV light, the strain at break becomes evidently larger. Moreover, since the stress increases with strain, the stress at break after UV irradiation also increases remarkably, though at the same strain the tensile stress of the irradiated P8 is smaller than that of the un-irradiated sample. As we can see, UV irradiation can greatly alter the tensile property of PMMAZO-*b*-PnBA-*b*-PMMAZO BCPs. The irradiated samples exhibit better elasticity but a lower tensile stress. This can be attributed to the isotropization of the LC phase induced by UV irradiation, which reduces the

strength and enhance the deformability of the physically cross-linking domains, i.e. PMMAZO domains. As a consequence, the mechanical properties of the PMMAZO-*b*-PnBA-*b*-PMMAZO BCPs are variable and photoresponsive, which means that this type of BCP can be potentially used as a smart and functional TPE.

4. Conclusions

The results show that the PMMAZO-*b*-PnBA-*b*-PMMAZO BCPs can self-assemble into hierarchical structures at different scales in the bulk, which are affected by the interplay between the LC ordering and microphase separation. On the one hand, the stacking of the LC moiety, the phase transition temperature and domain size of the LC phase are dependent on the microphase-separated structure. On the other hand, for the BCP with a specific composition, isotropization of the LC phase may also cause an OOT of the microphase-separated structure and the *d*-spacing of the microphase-separated structure may change along with the LC phase transitions. Moreover, isomerization of the azobenzene LC moieties can be triggered by UV irradiation, leading to a lower density of the LC phase. This will further alter the microphase separation behavior of the BCPs, including decrease in the regularity of the microphase-separated structure and occurrence of OOT. The tensile property of the triblock copolymers also varies with UV irradiation. Larger elasticity is yielded after UV irradiation.

Acknowledgements

This work was supported by the National Basic Research Program of China (973 Program) (2011CB606005) and the National Natural Science Foundation of China (51073138). The authors would also like to thank beamlines BL16B1 and BL14B1 (Shanghai Synchrotron Radiation Facility) for providing the beam time.

Notes and references

1 I. W. Hamley, *The Physics of Block Copolymers*. Oxford University Press: 1998.
2 W. N. He and J. T. Xu, *Prog. Polym. Sci.*, 2012, **37**, 1350-1400.
3 M. W. Matsen and F. S. Bates, *Macromolecules*, 1996, **29**, 1091-1098.
4 D. G. Bucknall and H. L. Anderson, *Science*, 2003, **302**, 1904-1905.
5 A. V. Ruzette and L. Leibler, *Nat Mater*, 2005, **4**, 19-31.
6 K. K. Tenneti, X. F. Chen, C. Y. Li, Y. F. Tu, X. H. Wan, Q. F. Zhou, I. Sics and B. S. Hsiao, *J. Am. Chem. Soc.*, 2005, **127**, 15481-15490.
7 H. F. Yu, T. Kobayashi and H. Yang, *Adv. Mater.*, 2011, **23**, 3337-3344.
8 L. Y. Shi, I. F. Hsieh, Y. Zhou, X. F. Yu, H. J. Tian, Y. Pan, X. H. Fan and Z. H. Shen, *Macromolecules*, 2012, **45**, 9719-9726.
9 Z. H. Shi, D. Z. Chen, H. J. Lu, B. Wu, J. Ma, R. S. Cheng, J. L. Fang and X. F. Chen, *Soft Matter*, 2012, **8**, 6174-6184.
10 H. Komiyama, R. Sakai, S. Hadano, S. Asaoka, K. Kamata, T. Iyoda, M. Komura, T. Yamada and H. Yoshida, *Macromolecules*, 2014, **47**, 1777-1782.
11 H. F. Yu and T. Kobayashi, *Molecules*, 2010, **15**, 570-603.
12 H. F. Yu, *Prog. Polym. Sci.*, 2014, **39**, 781-815.
13 L. Leibler, *Macromolecules*, 1980, **13**, 1602-1617.
14 A. K. Khandpur, S. Förster, F. S. Bates, I. W. Hamley, A. J. Ryan, W. Bras, K. Almdal and K. Mortensen, *Macromolecules*, 1995, **28**, 8796-8806.
15 M. Walther and H. Finkelmann, *Prog. Polym. Sci.*, 1996, **21**, 951-979.
16 S. Poser, H. Fischer and M. Arnold, *Prog. Polym. Sci.*, 1998, **23**, 1337-1379.
17 M. Lee, B. K. Cho and W. C. Zin, *Chem. Rev.*, 2001, **101**, 3869-3892.
18 M. Anthamatten and P. T. Hammond, *Macromolecules*, 1999, **32**, 8066-8076.
19 Y. Zhao, B. Qi, X. Tong and Y. Zhao, *Macromolecules*, 2008, **41**, 3823-3831.
20 H. L. Xie, Y. X. Liu, G. Q. Zhong, H. L. Zhang, E. Q. Chen and Q. F. Zhou, *Macromolecules*, 2009, **42**, 8774-8780.
21 P. Deshmukh, S. K. Ahn, L. G. de Merxem and R. M. Kasi, *Macromolecules*, 2013, **46**, 8245-8252.
22 P. Deshmukh, S. K. Ahn, M. Gopinadhan, C. O. Osuji and R. M. Kasi, *Macromolecules*, 2013, **46**, 4558-4566.
23 F. Zhou, T. Y. Ye, L. Y. Shi, C. Xie, S. K. Chang, X. H. Fan and Z. H. Shen, *Macromolecules*, 2013, **46**, 8253-8263.
24 C. O. Osuji, J. T. Chen, G. Mao, C. K. Ober and E. L. Thomas, *Polymer*, 2000, **41**, 8897-8907.
25 I. W. Hamley, V. Castelletto, Z. B. Lu, C. T. Imrie, T. Itoh and M. Al-Hussein, *Macromolecules*, 2004, **37**, 4798-4807.
26 I. W. Hamley, V. Castelletto, P. Parras, Z. B. Lu, C. T. Imrie and T. Itoh, *Soft Matter*, 2005, **1**, 355-363.
27 H. C. Kim, S. M. Park and W. D. Hinsberg, *Chem. Rev.*, 2009, **110**, 146-177.
28 H. Takeshita, S. I. Taniguchi, M. Arimoto, M. Miya, K. Takenaka and T. Shiomi, *Polymer*, 2009, **50**, 271-278.
29 A. Schneider, J. J. Zanna, M. Yamada, H. Finkelmann and R. Thomann, *Macromolecules*, 2000, **33**, 649-651.
30 G. P. Mao, J. G. Wang, C. K. Ober, M. Brehmer, M. J. O'Rourk and E. L. Thomas, *Chem. Mater.*, 1998, **10**, 1538-1545.
31 J. Sänger, W. Gronski, S. Maas, B. Stühn and B. Heck, *Macromolecules*, 1997, **30**, 6783-6787.
32 W. Y. Zheng and P. T. Hammond, *Macromolecules*, 1998, **31**, 711-721.
33 Y. Guan, X. F. Chen, H. Y. Ma, Z. H. Shen and X. H. Wan, *Soft Matter*, 2010, **6**, 922-927.
34 M. Anthamatten, J. S. Wu and P. T. Hammond, *Macromolecules*, 2001, **34**, 8574-8579.
35 B. D. Olsen and R. A. Segalman, *Macromolecules*, 2005, **38**, 10127-10137.
36 B. D. Olsen and R. A. Segalman, *Macromolecules*, 2007, **40**, 6922-6929.

37 L. Y. Shi, Z. H. Shen and X. H. Fan, *Macromolecules*, 2011, **44**, 2900-2907.
38 L. Cui, X. Tong, X. Yan, G. Liu and Y. Zhao, *Macromolecules*, 2004, **37**, 7097-7104.
39 Y. Q. Tian, K. Watanabe, X. X. Kong, J. Abe and T. Iyoda, *Macromolecules*, 2002, **35**, 3739-3747.
40 M. Häckel, L. Kador, D. Kropp, C. Frenz and H. W. Schmidt, *Adv. Funct. Mater.*, 2005, **15**, 1722-1727.
41 H. F. Yu, K. Okano, A. Shishido, T. Ikeda, K. Kamata, M. Komura and T. Iyoda, *Adv. Mater.*, 2005, **17**, 2184-2188.
42 A. Saishoji, D. Sato, A. Shishido and T. Ikeda, *Langmuir*, 2006, **23**, 320-326.
43 H. F. Yu, J. Li, T. Ikeda and T. Iyoda, *Adv. Mater.*, 2006, **18**, 2213-2215.
44 T. Breiner, K. Kreger, R. Hagen, M. Häckel, L. Kador, A. H. E. Müller, E. J. Kramer and H. W. Schmidt, *Macromolecules*, 2007, **40**, 2100-2108.
45 T. Ikeda, *J. Mater. Chem.*, 2003, **13**, 2037-2057.
46 H. F. Yu and T. Ikeda, *Adv. Mater.*, 2011, **23**, 2149-2180.
47 H. F. Yu, T. Iyoda, K. Okano, A. Shishido and T. Ikeda, *Mol. Cryst. Liq. Cryst.*, 2005, **443**, 191-199.
48 Y. Zhao and J. He, *Soft Matter*, 2009, **5**, 2686-2693.
49 Y. Zhu and X. G. Wang, *Acta Polym. Sin.*, 2013, **0**, 962-970.
50 T. Seki, *Macromol. Rapid Commun.*, 2014, **35**, 271-290.
51 W. Chen, J. Y. Wang, X. Wei, J. Xu, A. C. Balazs, K. Matyjaszewski and T. P. Russell, *Macromolecules*, 2011, **44**, 278-285.
52 W. Chen, X. Wei, A. C. Balazs, K. Matyjaszewski and T. P. Russell, *Macromolecules*, 2011, **44**, 1125-1131.
53 H. F. Yu, T. Iyoda and T. Ikeda, *J. Am. Chem. Soc.*, 2006, **128**, 11010-11011.
54 M. H. Li, P. Keller, B. Li, X. Wang and M. Brunet, *Adv. Mater.*, 2003, **15**, 569-572.
55 Y. Yu, M. Nakano and T. Ikeda, *Nature*, 2003, **425**, 145-145.
56 H. K. Kim, X. S. Wang, Y. Fujita, A. Sudo, H. Nishida, M. Fujii and T. Endo, *Macromol. Chem. Phys.*, 2005, **206**, 2106-2111.
57 H. Y. Wen, W. D. Zhang, Y. Y. Weng and Z. J. Hu, *RSC Advances*, 2014, **4**, 11776-11781.
58 H. Ringsdorf and H. W. Schmidt, *Makromol. Chem.*, 1984, **185**, 1327-1334.
59 H. L. Xie, S. J. Wang, G. Q. Zhong, Y. X. Liu, H. L. Zhang and E. Q. Chen, *Macromolecules*, 2011, **44**, 7600-7609.
60 W. Deng, P. A. Albouy, E. Lacaze, P. Keller, X. Wang and M. H. Li, *Macromolecules*, 2008, **41**, 2459-2466.
61 A. J. Meuler, C. J. Ellison, J. Qin, C. M. Evans, M. A. Hillmyer and F. S. Bates, *J. Chem. Phys.*, 2009, **130**, 234903.
62 A. K. Schmitt and M. K. Mahanthappa, *Macromolecules*, 2014, **47**, 4346-4356.
63 J. T. Xu, L. Xue, Z. Q. Fan, Z. H. Wu and J. K. Kim, *Macromolecules*, 2006, **39**, 2981-2988.
64 Y. J. Qiu, J. T. Xu, L. Xue, Z. Q. Fan and Z. H. Wu, *J. Appl. Polym. Sci.*, 2007, **103**, 2464-2471.
65 M. Walther, H. Faulhammer and H. Finkelmann, *Macromol. Chem. Phys.*, 1998, **199**, 223-237.
66 Y. Zhao, B. Qi, X. Tong and Y. Zhao, *Macromolecules*, 2008, **41**, 3823-3831.
67 X. Tong, L. Cui and Y. Zhao, *Macromolecules*, 2004, **37**, 3101-3112.
68 P. Ravi, S. L. Sin, L. H. Gan, Y. Y. Gan, K. C. Tam, X. L. Xia and X. Hu, *Polymer*, 2005, **46**, 137-146.